

NRC Publications Archive Archives des publications du CNRC

Local structure and first cycle redox mechanism of layered $\text{Li}_{1.2}\text{Cr}_{0.4}\text{Mn}_{0.4}\text{O}_2$ cathode material

Ammundsen, Brett; Paulsen, Jens; Davidson, Isobel; Liu, Ru-Shi; Shen, Chih-Hung; Chen, Jin-Ming; Jang, Ling-Yun; Lee, Jyh-Fu

This publication could be one of several versions: author's original, accepted manuscript or the publisher's version. / La version de cette publication peut être l'une des suivantes : la version prépublication de l'auteur, la version acceptée du manuscrit ou la version de l'éditeur.

For the publisher's version, please access the DOI link below. / Pour consulter la version de l'éditeur, utilisez le lien DOI ci-dessous.

Publisher's version / Version de l'éditeur:

<https://doi.org/10.1149/1.1456535>

Journal of the Electrochemical Society, 149, February 4, pp. A431-A436, 2002

NRC Publications Archive Record / Notice des Archives des publications du CNRC :

<https://nrc-publications.canada.ca/eng/view/object/?id=5af78c3b-617f-464e-b034-46904ddfa948>

<https://publications-cnrc.canada.ca/fra/voir/objet/?id=5af78c3b-617f-464e-b034-46904ddfa948>

Access and use of this website and the material on it are subject to the Terms and Conditions set forth at

<https://nrc-publications.canada.ca/eng/copyright>

READ THESE TERMS AND CONDITIONS CAREFULLY BEFORE USING THIS WEBSITE.

L'accès à ce site Web et l'utilisation de son contenu sont assujettis aux conditions présentées dans le site

<https://publications-cnrc.canada.ca/fra/droits>

LISEZ CES CONDITIONS ATTENTIVEMENT AVANT D'UTILISER CE SITE WEB.

Questions? Contact the NRC Publications Archive team at

PublicationsArchive-ArchivesPublications@nrc-cnrc.gc.ca. If you wish to email the authors directly, please see the first page of the publication for their contact information.

Vous avez des questions? Nous pouvons vous aider. Pour communiquer directement avec un auteur, consultez la première page de la revue dans laquelle son article a été publié afin de trouver ses coordonnées. Si vous n'arrivez pas à les repérer, communiquez avec nous à PublicationsArchive-ArchivesPublications@nrc-cnrc.gc.ca.



Local Structure and First Cycle Redox Mechanism of Layered $\text{Li}_{1.2}\text{Cr}_{0.4}\text{Mn}_{0.4}\text{O}_2$ Cathode Material

Brett Ammundsen,^{a,*} Jens Paulsen,^{a,*} Isobel Davidson,^{b,*} Ru-Shi Liu,^c
Chih-Hung Shen,^c Jin-Ming Chen,^d Ling-Yun Jang,^d and Jyh-Fu Lee^d

^aPacific Lithium (New Zealand) Limited, Auckland, New Zealand

^bNational Research Council Canada, Institute for Chemical Process and Environmental Technology, Ottawa, Ontario, Canada K1A 0R6

^cDepartment of Chemistry, National Taiwan University, Taipei, Taiwan

^dSynchrotron Radiation Research Center, Hsinchu, Taiwan

Electrochemical, X-ray diffraction, and K and L edge X-ray absorption data are reported for the layered cathode material $\text{Li}_{1.2}\text{Mn}_{0.4}\text{Cr}_{0.4}\text{O}_2$. The structural data show that this material can be understood as a solid solution of the layered phases Li_2MnO_3 and LiCrO_2 , comprising tetravalent Mn and trivalent Cr, with approximately 0.2 lithium incorporated in the transition metal layers. According to the analysis of the K edge extended X-ray absorption fine structure, lithium ions in the transition metal layers are clustered around Mn ions. L edge X-ray absorption near edge spectra show that in the first charge-discharge cycle chromium is the electrochemically active species, cycling between Cr^{3+} and Cr^{6+} . Manganese remains as Mn^{4+} throughout charge and discharge.

© 2002 The Electrochemical Society. [DOI: 10.1149/1.1456535] All rights reserved.

Manuscript submitted September 25, 2001; revised manuscript received October 29, 2001. Available electronically February 25, 2002.

Layered lithium manganese oxides are of interest as cathodes for rechargeable lithium batteries due to the safety, low cost, and low toxicity of manganese-based materials. However, basic problems such as the collapse of the layer structure toward the spinel structure have not yet been solved. This collapse usually leads to poor rate performance and to evolution of a two-plateau voltage profile, both of which are undesirable for practical applications.¹

Recently the development of a novel layered oxide cathode material, $\text{Li}_{1.2}\text{Cr}_{0.4}\text{Mn}_{0.4}\text{O}_2$, was reported, showing high capacity and good cycling stability in lithium-ion cells.² The material belongs to the solid solution series $\text{Li}_{2+x}\text{Cr}_y\text{Mn}_{2-y}\text{O}_{4+\delta}$ first reported by Davidson *et al.*,^{3,4} corresponding to the formulation $\text{Li}_3\text{CrMnO}_5$ using the notation given by Davidson *et al.* (in the present work we prefer to use the notation $\text{Li}_{1.2}\text{Cr}_{0.4}\text{Mn}_{0.4}\text{O}_2$ because it relates better to the rock salt crystal structure, as discussed below). Davidson *et al.* have evaluated the solid solution range in $\text{Li}_{2+x}\text{Cr}_y\text{Mn}_{2-y}\text{O}_{4+\delta}$ from $y = 0.49$ to $y = 1.46$, and found that discharge capacity tends to increase with higher Cr/Mn ratio, up to 230 mAh/g.³ Although lower Cr/Mn ratios gave lower capacities, high reversible capacities of up to 200 mAh/g were found in examples with a Cr/Mn ratio of around 1.0.

The objective of the work reported here is to examine in greater detail the structure and electrochemistry of the $\text{Li}_{1.2}\text{Cr}_{0.4}\text{Mn}_{0.4}\text{O}_2$ material. We are interested in this phase because the composition has shown high capacity and yet contains 50% of its transition metal content as Mn. During the first charge of this material, up to 270 mAh/g (corresponding to nearly 1 Li in $\text{Li}_{1.2}\text{Cr}_{0.4}\text{Mn}_{0.4}\text{O}_2$) can be extracted. This is only possible if either side reactions occur or the average transition metal valence state in the charged cathode is higher than the expected tetravalent state. The work reported here uses a combination of X-ray diffraction, and X-ray absorption at the transition metal K and L edges, to investigate the crystal and electronic structure of $\text{Li}_{1.2}\text{Cr}_{0.4}\text{Mn}_{0.4}\text{O}_2$, as prepared and during the first charge-discharge cycle. X-ray diffraction (XRD) gives information about the long range order. X-ray absorption spectroscopy (XAS) provides independent local structural information for the manganese and chromium coordination environments, including information about the oxidation state. Together these methods allow a full description of the structure and redox processes occurring during the first cycle to be given.

Experimental

Sample preparation.— $\text{Li}_{1.2}\text{Cr}_{0.4}\text{Mn}_{0.4}\text{O}_2$ was prepared by reacting stoichiometric amounts of coprecipitated mixed hydroxides of chromium and manganese with lithium carbonate at 800°C for 10 h under flowing argon. Inductively coupled plasma (ICP) analysis of the chemical composition gave $\text{Li}_{1.17}\text{Cr}_{0.41}\text{Mn}_{0.42}\text{O}_2$, close to the target stoichiometry.

For the XAS experiments samples of LiCrO_2 , Li_2MnO_3 , and monoclinic $\text{LiCr}_{0.10}\text{Mn}_{0.90}\text{O}_2$ were prepared as model compounds for Cr^{3+} , Mn^{4+} , and Mn^{3+} , respectively, in layer-type rock salt crystal environments. LiCrO_2 and Li_2MnO_3 were prepared by solid-state reactions, reacting stoichiometric amounts of lithium carbonate with Cr_2O_3 (20 h at 800°C in air), and MnO_2 (20 h at 800°C in air) respectively. $\text{LiCr}_{0.10}\text{Mn}_{0.90}\text{O}_2$ was prepared as described in an earlier work.⁵

X-ray diffraction.—Powder XRD data were collected on a Philips X'Pert diffractometer using $\text{Cu K}\alpha$ radiation. Rietveld refinement of the data was carried out using Fullprof⁶ software.

Electrochemical testing and preparation of cathodes for ex situ measurements.—For the electrochemical cycling and ex situ XRD and XAS measurements, cathodes comprising the $\text{Li}_{1.2}\text{Cr}_{0.4}\text{Mn}_{0.4}\text{O}_2$ powder + carbon black + poly(vinylidene fluoride) in 80:12:8 weight ratio were coated on an aluminum foil current collector. Cathodes were assembled in coin cells together with lithium metal foil anodes, glass fiber separators, and 1 M LiPF_6 in (50 w/w ethylene carbonate + 50 w/w dimethylene carbonate) electrolyte solution, under a dry (<1 ppm H_2O) argon atmosphere. An Arbin series BT2043 automated battery charging system was used to cycle the cells.

For the ex situ experiments, cells were charged and discharged at 10 mA/g to the desired voltage, and allowed to equilibrate for 40 h before opening the cells to recover the cathodes. The cathodes were rinsed with diethyl carbonate and stored in dry sealed containers until the X-ray absorption near-edge structure (XANES) measurements.

X-ray absorption experiments.—XAS experiments were carried out at the Synchrotron Radiation Research Center (SRRC), Hsinchu, Taiwan. All data were collected at room temperature. Cr and Mn K edge data were recorded in transmission mode on as-synthesized powder mounted on Scotch tape, at the BL17C Wiggler beamline using a double-crystal Si(111) monochromator. The higher X-ray

* Electrochemical Society Active Member.

^z E-mail: brett@pacificlithium.co.nz

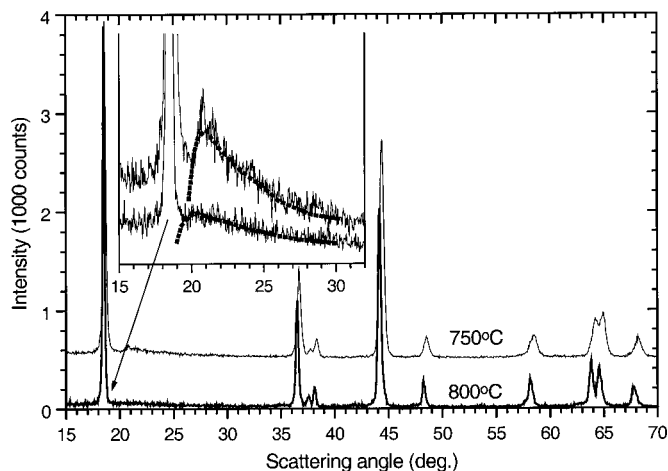


Figure 1. Powder XRD pattern of $\text{Li}_{1.2}\text{Cr}_{0.4}\text{Mn}_{0.4}\text{O}_2$ annealed at 800°C for 10 h and, for comparison, annealed at 750°C . (Inset shows buckle corresponding to short-range Li ordering in transition metal layers.)

harmonics were rejected by mirrors. The spectra were scanned from 5.8 to 7.5 keV using a gas-ionization detector. The ion chambers used for measuring the incident (I_0) and transmitted (I) beam intensities were filled with a mixture of N_2 and He gases and a mixture of N_2 and Ar gases, respectively. The energy scales were calibrated by monitoring with Cr and Mn foils. Data were normalized and analyzed using the extended X-ray absorption fine structures (EXAFS) programs of Michalowicz,⁷ following procedures described previously.⁸

XANES measurements.—These measurements at the Cr and Mn L_{23} edges were performed directly on the cathode films, on the 6 m high-energy spherical grating monochromator (HSGM) beamline. Samples were put into an ultrahigh vacuum chamber (10^{-9} Torr) in order to avoid surface contamination. The XANES spectra were recorded by the sample drain current mode at room temperature. The incident photon flux (I_0) was monitored simultaneously by a Ni mesh located after the exit slit of the monochromator. All X-ray absorption spectra were normalized to I_0 . The photon energies were calibrated within an accuracy of ~ 0.1 eV using known absorption peaks of CuO.

Results

X-ray diffraction.—Figure 1 shows the powder XRD pattern of the $\text{Li}_{1.2}\text{Cr}_{0.4}\text{Mn}_{0.4}\text{O}_2$ material. For comparison a pattern of a sample prepared at lower temperature (750°C) is added. The inset enlarges the region between 15 and $32^\circ 2\theta$. In this region a buckle appears, more or less pronounced depending on the annealing temperature. Figure 2 shows the X-ray data together with the calculated pattern and the difference between the calculated and observed patterns. The pattern can be indexed in the $R\bar{3}m$ space group. The unit cell parameters for the hexagonal cell are $a = 2.886$ Å and $c = 14.372$ Å. The Rietveld refinement delivers $\{\text{Li}_{1-x}\text{M}_x\}_{3b}[\text{Li}_y\text{M}_{1-y}]_{3a}(\text{O}_2)_{6c}$ with $x \cong 0$ ($x = -0.01$) and $y = 0.16$. Thus the layer structure consists of lithium layers (3b sites) alternating with transition metal/lithium layers (3a sites), separated by oxygen layers. M was fixed as $\text{M} = [\text{Cr}_{1/2}\text{Mn}_{1/2}]$.

The crystal structure is similar to that of other layered lithium transition metal oxides such as LiCoO_2 (which is $\{\text{Li}\}_{3b}[\text{Co}]_{3a}(\text{O}_2)_{6c}$), with the significant distinction that $\text{Li}_{1.2}\text{Cr}_{0.4}\text{Mn}_{0.4}\text{O}_2$ has additional lithium incorporated in the transition metal layers. Lithium and transition metal ions have very different scattering powers so that an ordering of Li and M in the transition metal layers would result in superstructure peaks.

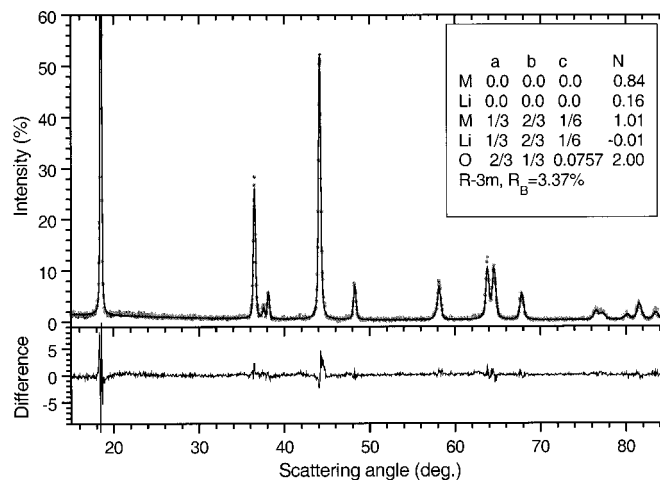


Figure 2. Comparison of calculated and observed XRD patterns of $\text{Li}_{1.2}\text{Cr}_{0.4}\text{Mn}_{0.4}\text{O}_2$ annealed at 800°C . The crystallographic data used for the calculation are given in the figure.

Li_2MnO_3 is a layered phase with $[\text{Li}_{1/3}\text{Mn}_{2/3}]$ long-range ordering in the transition metal layers, resulting in a series of well-resolved superstructure peaks located in the region 21 to $32^\circ 2\theta$. In the XRD pattern of $\text{Li}_{1.2}\text{Cr}_{0.4}\text{Mn}_{0.4}\text{O}_2$ a broad buckle is present in this same region, indicating that similar near-ordering correlations are present as in Li_2MnO_3 , but more diffuse at long range.

From the lattice constants a c/a ratio of 4.979 is calculated. A c/a ratio of 4.90 corresponds to cubic lattice constants. The more the c/a ratio deviates from 4.90, the better is the layer character. It can be concluded that $\text{Li}_{1.2}\text{Cr}_{0.4}\text{Mn}_{0.4}\text{O}_2$ has a pronounced layer structure. The c/a ratio approaches that of well-layered LiCoO_2 (4.99), and is higher than that of LiNiO_2 (typically around 4.93).

K edge XANES.—In general, the shape of K edge XANES spectra of transition metals in oxides is sensitive to the local structural environment of the element, while the threshold energy position of the absorption edge is sensitive to oxidation state. Figure 3A shows the XANES spectrum for $\text{Li}_{1.2}\text{Cr}_{0.4}\text{Mn}_{0.4}\text{O}_2$ at the Cr K edge, compared with the spectrum for layered LiCrO_2 . The two spectra are practically identical, indicating that the Cr environments in the two compounds are similar. It can be concluded that chromium in $\text{Li}_{1.2}\text{Cr}_{0.4}\text{Mn}_{0.4}\text{O}_2$ is trivalent and in octahedral sites similar to LiCrO_2 .

Figure 3B shows the XANES spectrum for $\text{Li}_{1.2}\text{Cr}_{0.4}\text{Mn}_{0.4}\text{O}_2$ at the Mn K edge, compared with spectra for Li_2MnO_3 and layered $\text{LiCr}_{0.10}\text{Mn}_{0.90}\text{O}_2$. Manganese is tetravalent and octahedrally surrounded by oxygen in Li_2MnO_3 , and trivalent with an octahedral environment distorted by Jahn-Teller stabilization in $\text{LiCr}_{0.10}\text{Mn}_{0.90}\text{O}_2$. The distorted octahedral environment in the latter compound gives rise to the broadened features in the XANES spectrum, while the lower oxidation state shifts the absorption edge threshold of Mn^{3+} to lower energy than that of Mn^{4+} . The comparison shows clearly that $\text{Li}_{1.2}\text{Cr}_{0.4}\text{Mn}_{0.4}\text{O}_2$ has tetravalent manganese in regular octahedral coordination similar to Li_2MnO_3 .

K edge EXAFS.—Analysis of K edge EXAFS data provides quantitative information about the local coordination environment of the target element. Figure 4 shows the Fourier-transformed EXAFS data recorded for $\text{Li}_{1.2}\text{Cr}_{0.4}\text{Mn}_{0.4}\text{O}_2$ at the Cr and Mn K edges. Table I gives the coordination numbers and interatomic distances for the first coordination shell of oxygen, and second coordination shell (in this compound corresponding to the occupancy of the six nearest-neighbor cation sites in the transition metal layer), around Cr and Mn, obtained by least-squares fitting of the EXAFS data. Data ob-

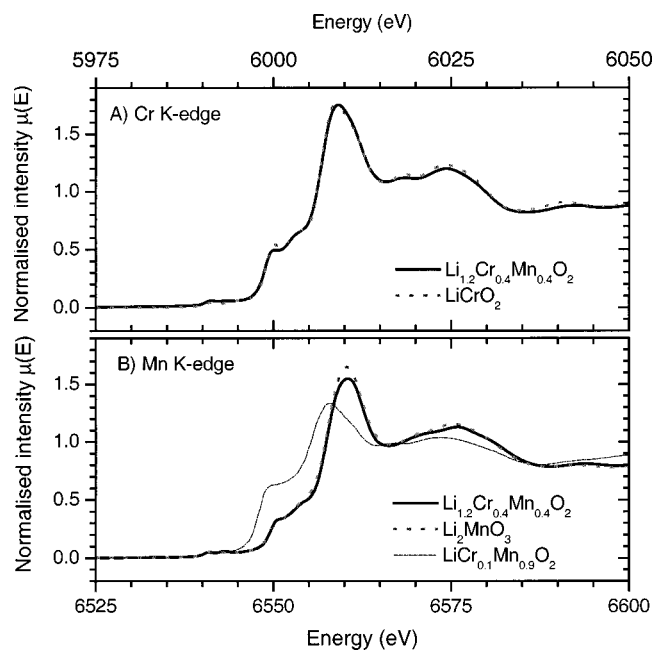


Figure 3. X-ray absorption near-edge spectra for $\text{Li}_{1.2}\text{Cr}_{0.4}\text{Mn}_{0.4}\text{O}_2$. (A) Cr K edge spectrum, compared with LiCrO_2 . (B) Mn K edge spectrum, compared with Li_2MnO_3 and $\text{LiCr}_{0.1}\text{Mn}_{0.9}\text{O}_2$.

tained from the K edge EXAFS spectra of LiCrO_2 and Li_2MnO_3 are also given for comparison. The Cr-O and Mn-O distances in $\text{Li}_{1.2}\text{Cr}_{0.4}\text{Mn}_{0.4}\text{O}_2$ correspond closely to those for Cr^{3+} in LiCrO_2 and Mn^{4+} in Li_2MnO_3 . We note that the Mn-O coordination environment determined by EXAFS for $\text{Li}_{1.2}\text{Cr}_{0.4}\text{Mn}_{0.4}\text{O}_2$ is clearly different from the Jahn-Teller distorted Mn-O coordination of Mn^{3+} in $\text{LiCr}_{0.10}\text{Mn}_{0.90}\text{O}_2$.⁵

The Cr-M and Mn-M distances in $\text{Li}_{1.2}\text{Cr}_{0.4}\text{Mn}_{0.4}\text{O}_2$ are practically identical to each other, and between the second coordination shell distances observed in LiCrO_2 and Li_2MnO_3 . This latter observation supports a single-phase solid solution of Cr and Mn in $\text{Li}_{1.2}\text{Cr}_{0.4}\text{Mn}_{0.4}\text{O}_2$. However an interesting discrepancy between the Cr and Mn data sets is observed in the number of nearest transition metal neighbors determined by the refinements. The difference is observable in the different intensities of the second peak (M-M distance) in the Fourier-transformed data. Six transition metal neigh-

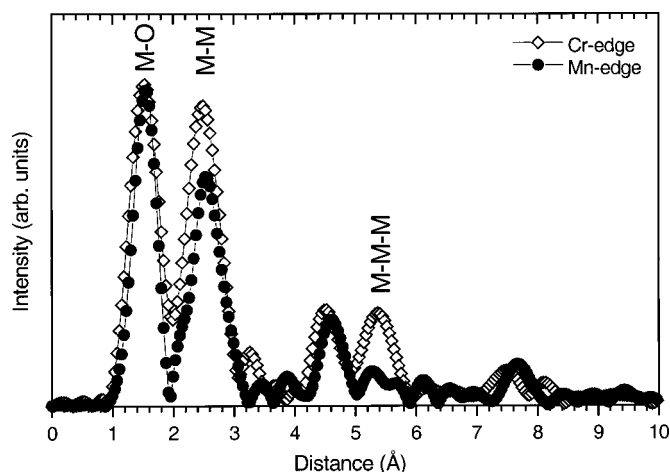


Figure 4. Fourier transformed EXAFS data for $\text{Li}_{1.2}\text{Cr}_{0.4}\text{Mn}_{0.4}\text{O}_2$ at the Mn and Cr K edges.

Table I. Structural parameters from EXAFS data: R is the interatomic distance between the absorbing and back-scattering atoms, N is the number of back-scattering atoms at this distance, and σ is the corresponding Debye-Waller factor for the coordination shell. Estimated uncertainties in R are ± 0.006 Å, and in N (where refined) ± 0.5 .

		R (Å)	N	σ (Å)
Li_2MnO_3	Mn-O	1.905	6 ^a	0.055
	Mn-Mn	2.837	4.5 ^a	0.073
$\text{Li}_{1.2}\text{Cr}_{0.4}\text{Mn}_{0.4}\text{O}_2$	Mn-O	1.904	6 ^a	0.059
	Mn-M	2.879	4.3	0.074
	Cr-O	1.972	6 ^a	0.059
	Cr-M	2.874	6.0	0.076
LiCrO_2	Cr-O	1.993	6 ^a	0.054
	Cr-Cr	2.892	6 ^a	0.063

^a Fixed parameters.

neighbors are expected in a perfect layered $\{\text{Li}\}_{3b}[\text{M}]_{3a}\text{O}_2$ phase. Additional lithium as in $\{\text{Li}\}_{3b}[\text{Li}_{0.2}\text{M}_{0.8}]_{3a}\text{O}_2$ should decrease this number. However full occupancy (all six sites occupied by Cr or Mn) was obtained when fitting the Cr data, whereas occupation of only around 4.5 out of the six sites was obtained for the Mn environment. This leads to a structural model in which the transition metal layers consist of localized clusters of $[\text{Li}_{1/3}\text{Mn}_{2/3}]$ and clusters of transition metal, predominantly chromium.

Further evidence for the local $[\text{Li}_{1/3}\text{Mn}_{2/3}]$ cluster model derives from the observation that the peak present in the Fourier-transformed Cr edge data at *ca.* 5.7 Å is much weaker in the Mn data. The distance corresponds to twice the nearest-neighbor cation distance, *i.e.*, to the next-nearest-neighbor Mn or Cr ion along the linear path formed by the edge-sharing MO_6 octahedra within the transition metal layers. The intensity of the peak in the Cr data is enhanced by a multiple scattering of the EXAFS photoelectron, a so-called focusing effect where the presence of the intermediary atom acts as a kind of lens.⁹ The coherence of this M-M-M interaction appears to be lost in the Mn data, consistent with local clusters of $[\text{Li}_{1/3}\text{Mn}_{2/3}]$ -type ordering. In Li_2MnO_3 the linear transition metal chains are interrupted by lithium, following the sequence M-M-Li-M-Li-M-Li...

Electrochemical testing and XRD of charged and discharged cathodes.—Figure 5 shows the first and second cycle charge-discharge voltage curves for $\text{Li}_{1.2}\text{Cr}_{0.4}\text{Mn}_{0.4}\text{O}_2$ between 4.4 and 2.5 V, cycling at a 7.5 mA/g current rate at 20°C. Like other compositions in the series reported by Davidson *et al.*,³ the first charge curve is different from subsequent charges and shows a large coulombic

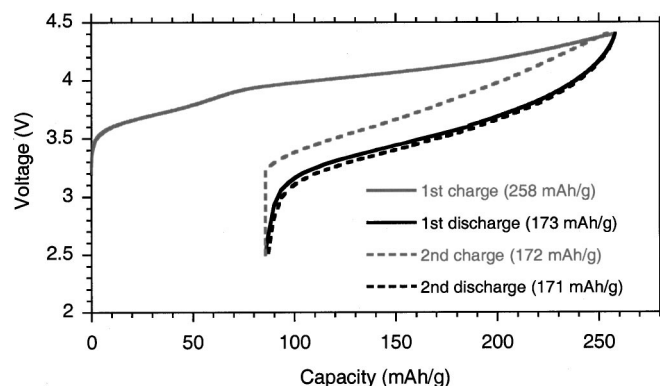


Figure 5. First and second cycle charge-discharge voltage curves for $\text{Li}_{1.2}\text{Cr}_{0.4}\text{Mn}_{0.4}\text{O}_2$ between 4.4 and 2.5 V (7.5 mA/g rate, 20°C).

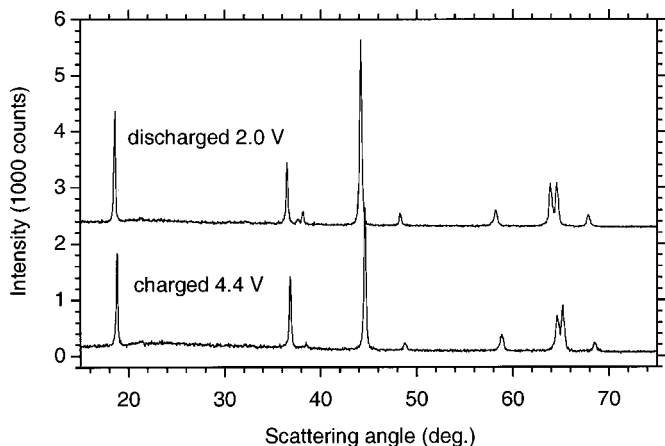


Figure 6. XRD patterns recorded for electrodes comprising $\text{Li}_{1.2}\text{Cr}_{0.4}\text{Mn}_{0.4}\text{O}_2$, extracted from Li button cells after first charge to 4.4 V and one full charge-discharge between 4.4 and 2.5 V.

irreversibility. Subsequent discharges are, however, the same as the first discharge, suggesting that no significant irreversible structural changes occur after the first cycle. Figure 6 shows XRD patterns recorded for cathodes extracted from cells after the first charge to 4.4 V, and after one full charge-discharge cycle between 4.4 and 2.5 V. Relative peak intensities are unreliable, particularly at lower angle, as a result of recording data on electrode films. Nonetheless the data show single phases with $R\bar{3}m$ symmetry for the cathode in both the charged and discharged state, with hexagonal cell parameters of $a = 2.863 \text{ \AA}$ and $c = 14.20 \text{ \AA}$, and $a = 2.886 \text{ \AA}$ and $c = 14.34 \text{ \AA}$, respectively. The overall structural framework and layered character of the material is therefore preserved through charge and discharge, although the c/a ratio decreases slightly in the charge process.

Figure 7 shows the results of extended cycling. Both at room temperature and 55°C the cathode material shows very good capacity retention. Figure 8 shows the discharge voltage profiles of the cells at current rates from C/5 (30 mA/g) to 2C (300 mA/g) measured from cycle 16 to 19, and from cycle 96 to 99. The voltage profiles remain stable, without evidence for the evolution of a double plateau around 4 V which typically appears in the discharge curves of layered manganese oxides as they undergo structural modification to spinel-related phases.¹ The appearance of a 4 V step in the discharge profiles of layered manganese oxides occurs when

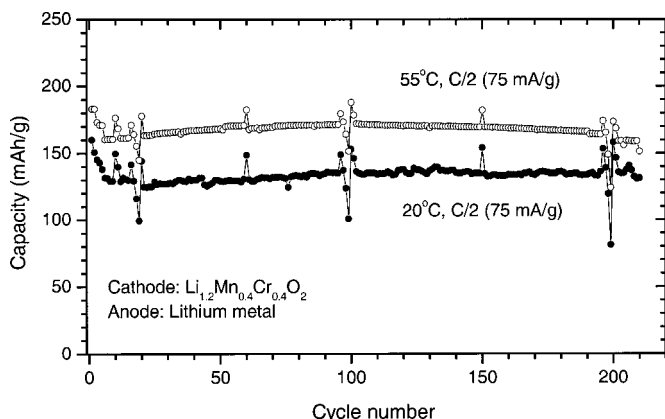


Figure 7. Extended cycling of $\text{Li}_{1.2}\text{Cr}_{0.4}\text{Mn}_{0.4}\text{O}_2$ at 20 and 55°C . The first five cycles used a C/5 (30 mA/g) rate, and thereafter a C/2 rate (75 mA/g) was used. Spikes are due to occasional measurements of rate capability and resistance using different rates.

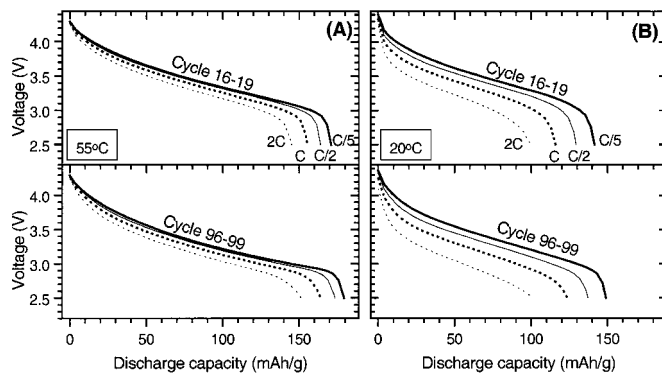


Figure 8. Voltage profiles of $\text{Li}_{1.2}\text{Cr}_{0.4}\text{Mn}_{0.4}\text{O}_2$ at different rates during the extended cycling tests of Fig. 7. (A) 55°C and (B) 20°C .

Mn ions migrate out of the transition metal layer leading to nucleation of spinel-like domains in the crystal structure with tetrahedral sites available for insertion of Li ions, as recently described by Reed *et al.*¹⁰ The absence of a 4 V step in the discharge profile of the $\text{Li}_{1.2}\text{Cr}_{0.4}\text{Mn}_{0.4}\text{O}_2$ material after extended cycling is therefore strong evidence for no significant formation of spinel-type phase.

L edge XANES.—Figure 9 (top) shows the Cr L edge XANES spectra recorded *ex situ* for electrodes comprising $\text{Li}_{1.2}\text{Cr}_{0.4}\text{Mn}_{0.4}\text{O}_2$, extracted from Li button cells after charge to 4.4 V, after charge to 4.4 V followed by discharge to 2.0 V, and after simple storage in the uncharged (pristine) state, compared with the spectrum for layered LiCrO_2 .

The Cr L edge spectrum for $\text{Li}_{1.2}\text{Cr}_{0.4}\text{Mn}_{0.4}\text{O}_2$ before charging matches well to that of Cr^{3+} in LiCrO_2 , confirming the conclusions from the K edge XAFS. After charging to 4.4 V, the basic spectrum of the LiCrO_2 -type structure is maintained (although with slightly lowered intensity), but an additional strong peak appears at around 579 eV. The latter peak corresponds to the energy position known for the $2p_{3/2}$ spectrum of Cr^{6+} .¹¹ XANES spectra recorded on cathodes at intermediate states of charge, 3.85 and 4.1 V (not shown in Fig. 9), show that the 579 eV peak appears early in the charge cycle and simply increases in intensity with increasing state of charge. During charge, therefore, Cr^{3+} is consumed and Cr^{6+} is formed. The mechanism is reversible. When the cathode is discharged to 2.0 V the 579 eV peak vanishes and the spectrum returns to that of trivalent Cr in the LiCrO_2 -type environment.

Figure 9 (bottom) compares the Mn L-edge spectra for the same cathodes as Fig. 9 (top), with the spectrum of Li_2MnO_3 . Again, the Mn spectrum of $\text{Li}_{1.2}\text{Cr}_{0.4}\text{Mn}_{0.4}\text{O}_2$ matches very well with that of Li_2MnO_3 , confirming the conclusions from the K edge XAFS that Mn is predominantly in a 4+ oxidation state. With charge and discharge the Mn L edge spectrum shows only small variations in the relative intensities of the different components of the multiplet, but no change in energy position. The small changes in relative intensities indicate some changes in the local structural environment, but no significant change in electronic state.

Discussion

XRD and EXAFS data together provide detailed information about the distribution of lithium, chromium, and manganese ions in $\text{Li}_{1.2}\text{Cr}_{0.4}\text{Mn}_{0.4}\text{O}_2$. From XRD, $\text{Li}_{1.2}\text{Cr}_{0.4}\text{Mn}_{0.4}\text{O}_2$ has a layered structure without transition metal located in the lithium layers. From the buckle at $21\text{--}32^\circ 2\theta$ in the diffraction data, together with the K edge EXAFS analysis, it can be concluded that lithium in the transition metal layers creates some diffuse ordering of the type observed in Li_2MnO_3 , forming local $[\text{Li}_{1/3}\text{Mn}_{2/3}]$ -like clusters. However the Li_2MnO_3 -type structure in $\text{Li}_{1.2}\text{Cr}_{0.4}\text{Mn}_{0.4}\text{O}_2$ is clearly at a short-range length scale, as it does not give rise to a discrete second

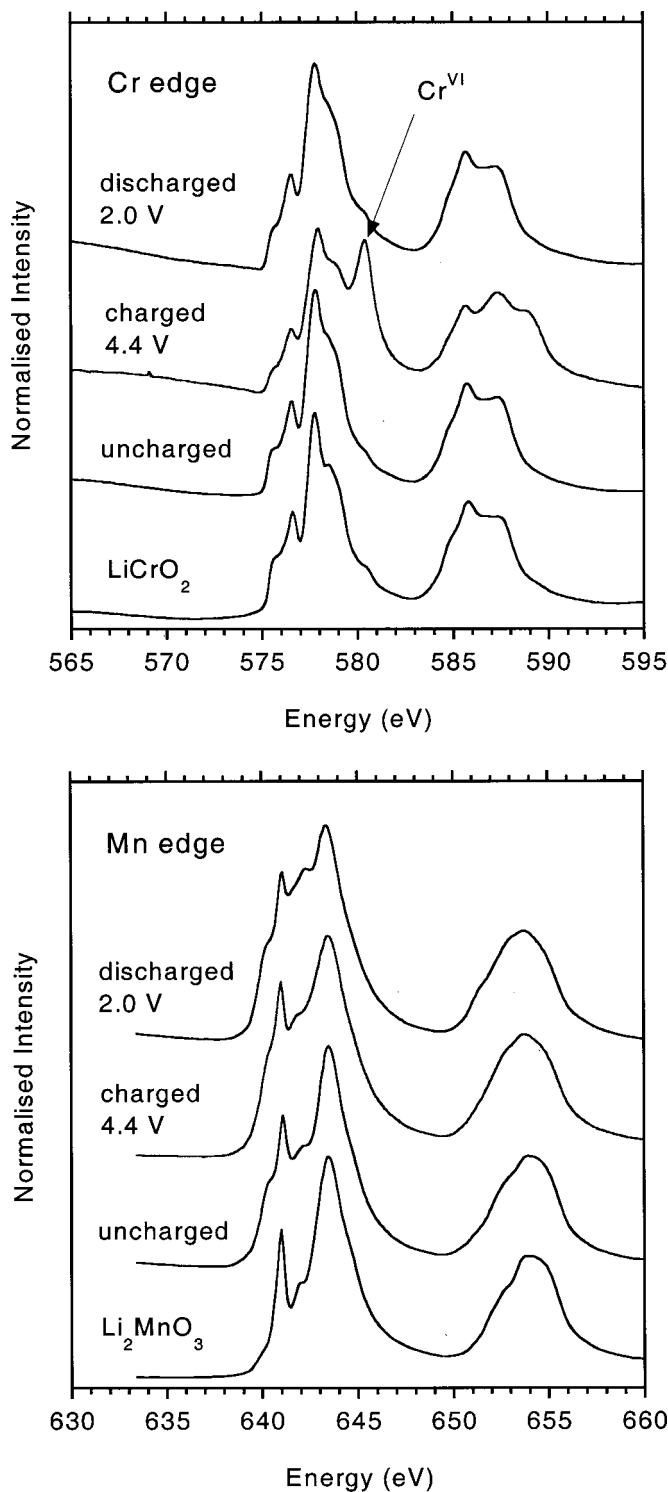


Figure 9. Cr (top) and Mn (bottom) L edge XAS recorded for electrodes comprising $\text{Li}_{1.2}\text{Cr}_{0.4}\text{Mn}_{0.4}\text{O}_2$ extracted from Li button cells, compared with LiCrO_2 (Cr) and Li_2MnO_3 (Mn).

phase by diffraction. The XRD pattern for $\text{Li}_{1.2}\text{Cr}_{0.4}\text{Mn}_{0.4}\text{O}_2$ shows the presence of a single phase with lattice parameters ($a = 2.886 \text{ \AA}$ and $c = 14.372 \text{ \AA}$) intermediate between Li_2MnO_3 ($a = 2.847 \text{ \AA}$, $c = 14.228 \text{ \AA}$, in the equivalent hexagonal cell) and LiCrO_2 ($a = 2.902 \text{ \AA}$, $c = 14.42 \text{ \AA}$), and is clearly distinguishable from the XRD pattern of a phase-separated mixture of the two compounds. The second shell Mn-(Mn/Cr) and Cr-(Mn/Cr) distances

determined by EXAFS (Table I) are also identical to each other within the uncertainties of the refinements, but different from the distances for either of the pure Li_2MnO_3 and LiCrO_2 phases, implying an intimate atomic level mixing of $[\text{Li}_{1/3}\text{Mn}_{2/3}]$ clusters and Cr ions in $\text{Li}_{1.2}\text{Cr}_{0.4}\text{Mn}_{0.4}\text{O}_2$. Intimate mixing rather than phase separation is clearly important for the electrochemical activity of the material. Neither Li_2MnO_3 nor LiCrO_2 are active as cathode materials, whereas $\text{Li}_{1.2}\text{Cr}_{0.4}\text{Mn}_{0.4}\text{O}_2$ may be cycled with high reversible capacity.

Local short-range ordering between Mn and Li in $\text{Li}_{1.2}\text{Cr}_{0.4}\text{Mn}_{0.4}\text{O}_2$ can be understood in terms of a simple application of Pauling's rule of electroneutrality to ordered rock salt phases.¹² In layered phases with mono-, tri-, and tetravalent cations, only $\text{LiM}^{3+}\text{O}_2$ and $\text{Li}[\text{M}_{1/3}^+\text{M}_{2/3}^{4+}]\text{O}_2$ stoichiometries can preserve local electroneutrality around oxygen. A complete disorder of Li, Mn, Cr in the transition metal layers, although preferred by entropy, would not conform to Pauling's rule.

The L edge X-ray absorption data demonstrate that the electrochemical oxidation and reduction of $\text{Li}_{1.2}\text{Cr}_{0.4}\text{Mn}_{0.4}\text{O}_2$ in the first cycle consists mainly of cycling of some part of the Cr between the trivalent and hexavalent states. To account for the capacity observed, approximately half of the Cr^{3+} in the compound would need to undergo this oxidation-reduction. There is no evidence in the Cr L edge spectra for Cr oxidation states intermediate between 3+ and 6+, *i.e.*, Cr^{4+} or Cr^{5+} , at any state of charge. A similar observation was made for Li insertion into Cr_3O_8 , using X-ray photoelectron spectroscopy (XPS).¹¹ Amorphous Cr_3O_8 has been shown to be cyclable over a limited range of approximately 1 Li per Cr, *i.e.*, around one-third of the Cr could be reversibly cycled between the hexavalent and trivalent states without capacity loss.¹¹

It is known that Cr^{3+} has a high stabilization energy for octahedral sites, but Cr^{6+} is only stable in tetrahedral sites. This implies that the Cr ions must reversibly migrate between octahedral and tetrahedral sites in the structure during charge and discharge. This would mean that lithium diffusion is coupled with a migration of chromium, which may account for the higher capacities obtained at 55°C relative to 20°C . The migration of Cr ions into tetrahedral sites during charge is difficult to determine with any precision from the XRD data of the charged cathode in Fig. 6, however structural evidence for reversible migration of Cr ions between octahedral and tetrahedral sites has been observed by *in situ* XAFS measurements.¹³ Surprisingly, the Cr migration does not have an adverse effect on the cycle life of the cathode, since $\text{Li}_{1.2}\text{Cr}_{0.4}\text{Mn}_{0.4}\text{O}_2$ has been cycled for more than 200 cycles at a C/2 charge and discharge rate with no serious loss of capacity.

As yet, it has not been possible to effectively stabilize O3 layered lithium manganese oxides, with manganese predominantly trivalent in the discharged state, against collapse toward spinel-type structure during cycling. The present results indicate that O3 layered phases with tetravalent manganese may present a different behavior.

Conclusions

The lithium-rich manganese chromium oxide $\text{Li}_{1.2}\text{Cr}_{0.4}\text{Mn}_{0.4}\text{O}_2$ may be prepared with a layered structure in which the additional lithium is incorporated in the transition metal layers. The structure can be understood as a solid solution of layered Li_2MnO_3 and LiCrO_2 , comprising tetravalent Mn and trivalent Cr with a local clustering of transition-metal-layer Li ions around Mn. Large amounts of lithium, translating to capacities near 200 mAh/g, can be reversibly extracted and intercalated. At least in the first cycle, Cr is the redox active species, cycling between Cr^{3+} and Cr^{6+} , embedded in an inert Li_2MnO_3 -like framework.

Pacific Lithium (New Zealand) Limited assisted in meeting the publication costs of this article.

References

1. B. Ammundsen and J. Paulsen, *Adv. Mater.*, **13**, 943 (2001).
2. B. Ammundsen, J. Desilvestro, R. Steiner, and P. Pickering, Abstract 17, The 10th International Meeting on Lithium Batteries, Como, Italy, May 28-June 2, 2000.
3. C. Storey, I. Kargina, Y. Grincourt, I. J. Davidson, Y. Yoo, and D. Y. Seung, *J. Power Sources*, **97-98**, 541 (2001).
4. Y. Gincourt, C. Storey, and I. J. Davidson, *J. Power Sources*, **97-98**, 711 (2001).
5. B. Ammundsen, J. Desilvestro, T. Groustou, D. Hassell, J. B. Metson, E. Regan, R. Steiner, and P. J. Pickering, *J. Electrochem. Soc.*, **147**, 4078 (2000).
6. J. Rodriguez-Carjaval, *Fullprof Manual*, Institut Laue-Langevin, Grenoble (1992).
7. A. Michalowicz, in *Logiciels pour la Chimie*, p. 102, Société Française de Chimie, Paris (1991).
8. B. Ammundsen, D. J. Jones, J. Rozière, and F. Villain, *J. Phys. Chem. B*, **102**, 7939 (1998).
9. B. Ammundsen, D. J. Jones, and J. Rozière, *J. Phys. IV*, **7**, C2 (1997).
10. J. Reed, G. Ceder, and A. Van Deren, *Electrochem. Solid-State Lett.*, **4**, A78 (2001).
11. O. Yamamoto, Y. Takeda, R. Kanno, Y. Oyabe, and Y. Shinya, *J. Power Sources*, **20**, 151 (1987).
12. G. C. Mather, C. Dussarrat, J. Etoumeau, and A. R. West, *J. Mater. Chem.*, **10**, 2219 (2000).
13. M. Balasubramanian, J. McBreen, I. J. Davidson, P. S. Whitfield, and I. Kargina, *J. Electrochem. Soc.*, **149**, A176 (2002).